International Journal of Bifurcation and Chaos, Vol. 15, No. 6 (2005) 1931–1944

FRICTION PAIR MODELING BY A 2-DOF SYSTEM: NUMERICAL AND EXPERIMENTAL INVESTIGATIONS

JAN AWREJCEWICZ and PAWEŁ OLEJNIK
Technical University of Lodz,
Department of Automatics and Biomechanics (K-16),
1/15 Stefanowskiego St., 90-924 Łódź, Poland

Received July 25, 2002; Revised April 30, 2003

A self-excited friction pair is modeled by a mechanical system of two degrees-of-freedom with a normal force varying during the block displacement. Two different friction coefficients are used, and a normal force pressing the sliding body to a belt depending on an angle bar motion of the analyzed system is applied. In addition, the numerical analysis is supported by the investigation of a real laboratory object modeling the feedback reinforcement of friction forces acting on the block. Both numerical and experimental results are compared showing good agreement.

Keywords: Stick-slip motion; numerical investigations; Lyapunov exponents; bifurcation diagrams; experimental friction; force model; laboratory rig.

1. Introduction

The nature of sliding components with an occurrence of intermittent stick and slip leads to unpredictable behaviors. These problems are exhibited in many industrial applications including bearings, disc brake systems, electric motor drives, rail mass transit systems, and machine tool/work piece systems [Ibrahim, 1992]. A fuller understanding of the stick-slip phenomena, which in consequence might help in elimination of its effects, is of considerable importance for applications requiring high precision motion [Armstrong-Hélouvry, 1992].

The relative sliding of two solid bodies is a nonequilibrium process where the kinetic energy of the motion is transferred into the energy of an irregular microscopic motion. This dissipative process is responsible for creation of a dry friction phenomenon. The phenomenological laws of dry friction, like Coulomb's laws, are well known and there is a well-established theory in the applied physics [Bowden & Tabor, 1954] related to this subject.

The simplest models describe friction as a function of the difference in the velocity of sliding bodies. Models such as the Coulomb's friction one are called static models. In fact, Coulomb's dry friction laws simplify a highly complex behavior that involves mechanical, plastic and chemical processes [Singer & Pollock, 1992]. Application of Coulomb's law often brings results that bear experimentally observable differences [Andreaus & Casini, 2001; Galvanetto *et al.*, 1995]. Computer simulations of mechanical systems with friction are complicated not only due to the strongly nonlinear behavior of the friction force near the zero velocity but also because of the lack of a universally considered friction model. For rigid bodies with dry friction, the classical Coulomb law of friction is usually applied in engineering contact problems exactly because of its simplicity. It can explain several phenomena associated with friction and it is commonly used for friction compensation [Friedland & Park, 1991].

A well-known velocity-limited friction model given by Oden and Martins [1985] uses a smooth quadratic function when the sliding velocity is near zero. However, although the value of the limiting velocity is essential here, there is no standard method for its estimation.

Using a different approach, Antunes *et al.* [1988] developed a spring-damper friction model that introduces both tangential spring and damper during sticking. The phase of motion is detected by a change in sign of the tangential velocity. The sticking spring force is expressed by a product of the adherence stiffness and contact distance from a zero tangential velocity. A viscous damper force is incorporated in parallel with the spring to damp out any residual numerical velocity.

Karnopp [1985] developed a force-balance model for one-dimensional motion with a small-velocity window. Outside the velocity window, the friction force may be any function of the sliding velocity. Inside the window, the friction force is estimated so as to balance the other forces in the system, the velocity remains small constant until the loss of the contact value of force is reached. This model has been used to describe many practical actuator and mechanism problems. Basing on Karnopp's model, Tan and Rogers [1996] developed a two-dimensional friction model often used for simulations of multi degrees-of-freedom systems with friction acting on a surface.

The problem of friction force modeling is not solved because the physics and dynamical effects are not sufficiently understood. There are two main theoretical approaches to the modeling of dry friction interfaces: the macro-slip and micro-slip ones [Feeny *et al.*, 1998; Singer & Pollock, 1992]. In the micro-slip approach, a relatively detailed analysis of the friction interfaces should be made. In this case, investigations can provide accurate results only when the preload between interfaces is very high. In the macro-slip approach, the entire surface is assumed to be either sliding or sticking. The force necessary to keep sliding at a constant velocity depends on the sliding velocity of the contact surfaces. With this respect, smooth and nonsmooth velocity-dependent friction laws have been cited in the references [Popp *et al.*, 1996; Oden & Martins, 1985; Makris & Constantinou, 1991].

Generally speaking, the various modifications of the Coulomb model, and the Karnopp model are all static in the sense that the friction model is a function of velocity. They can be substituted when friction is recognized to be in fact a dynamic phenomenon that should be modeled as a dynamical system. Under this convention, some of the dynamical dry friction models need to be specified: Dahl's models [Dahl, 1976]; Bliman-Sorine model [Bliman & Sorine, 1995]; LuGre model [Canudas de Vit *et al.*, 1995; Altpeter *et al.*, 1998].

There is an essential shortage of works that take into account modeling problems connected with the experimentally observable velocity-dependent friction force. The paper [Brandl & Pfeiffer, 1999] deals with measurement of dry friction. A tribometer was developed to identify both sticking and sliding friction coefficients. The so-called Stribeck-curve was determined for any material in the contact zone. Similarly, a multi degrees-of-freedom model of friction was investigated in [Bogacz & Ryczek, 1997], where an experimentally observable friction characteristic expressed the kinetic friction force as a function of the relative velocity of motion. The experimental investigation of vibrations of a system composed of a steel-polyester pair confirmed that the friction static force increases with both the increasing adhesion time and the growing force. Additionally, the kinetic friction force depends also on the sign of acceleration.

Despite numerous papers concerned with the analysis of regular and chaotic dynamics of mechanical systems with friction, not all possible nonlinear phenomena seem to have been properly understood or even detected and explained [Awrejcewicz, 1996; Awrejcewicz & Delfs, 1990a, 1990b; Brogliato, 1996; Galvanetto *et al.*, 1995; Kunze, 2000; Monteiro, 1994; Oden & Martins, 1985]. Although this paper is devoted to numerical and experimental investigations, the problem is expected to be attacked also from an analytical point of view. The stick-slip chaos has been predicted analytically using the Melnikov technique by Awrejcewicz and Holicke [1999], but such a prediction for a two degrees-of-freedom system is in general more complicated. Even if this problem has been solved, it will contain only a special type of nonlinear terms and will be valid only for special systems. Therefore, in this paper we have focused on numerical simulations, which are free from the mentioned drawbacks.

A self-excited system with friction analyzed in this work requires a suitable algorithm to avoid the problems that occur under integration of equations of motion with the sgn function and result in sudden jumps and undesired errors. In what follows, the Hénon method [Hénon, 1982; Awrejcewicz & Olejnik, 2002] is applied, which is particularly useful for obtaining suitable uniform solutions of nonsmooth systems (here with friction).

Estimation of Lyapunov exponents plays a crucial role in the analysis and identification of chaotic

dynamics. The estimation belongs to the fundamental tools [Wolf *et al.*, 1985; Van Wyk & Steeb, 1997] that allow learning about regularity of an attractor under analysis. At present, however, a novel approach, especially suitable for estimation of the Lyapunov exponents of nonsmooth systems, i.e. including those with friction, is applied.

2. The Modeled System with Friction

The study and prevention of unstable vibration of systems with friction is of essential importance in industry and there is a need for the friction pair modeling that could provide a correct description of the kinetic and static friction forces change between two moveable surfaces. The model can be further developed to govern also the dynamics of a brake mechanism [Awrejcewicz & Olejnik, 2003]. Therefore, the 2-DOF dynamical system illustrated schematically in Fig. 1 is analyzed numerically and investigated experimentally.

The self-excited system presented in Fig. 1 is equivalent to a real experimental rig in which *block* mass m is moving on the *belt* in x_1 direction, and where the *angle body* represented by moment mass of inertia J is rotating around point s with respect to angle direction ϕ. The analyzed system consists of the following parts: two bodies are coupled by linear springs k_2 and k_3; the block on the belt is additionally coupled to a fixed base by means of a linear spring k_1; the angle body is excited only by spring forces; there are no extra mechanical actuators; rotational motion of the angle body is damped using virtual actuators characterizing air resistance and denoted by constants c_1 and c_2; damping of the block is neglected; it is assumed that the angle of rotation of the angle body is small and within the interval $[+5, -5]$ degrees (in this case, rotation is equivalent to linear displacement y_1 of legs a of the angle body); the belt is moving with constant velocity v_b and there is no deformation of the belt in the contact zone.

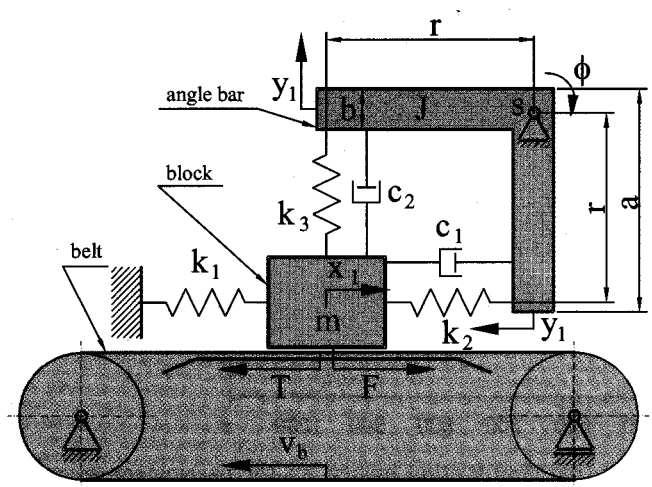

Fig. 1. The 2-DOF system under analysis.

Nondimensional equations that govern the dynamics of the system under investigation have the following form:

$$\begin{aligned} \dot{x}_1 &= x_2, \\ \dot{x}_2 &= -x_1 - \alpha_1^{-1}[\eta_1(x_2 + y_2) - y_1 - T], \\ \dot{y}_1 &= y_2, \\ \dot{y}_2 &= \alpha_2^{-1}(-\beta_3 y_1 - \eta_{12} y_2 - x_1 - \eta_1 x_2), \end{aligned} \tag{1}$$

where x_2, y_2, are velocities of the block and angle body, respectively; $v_{\rm rel} = x_2 - v_b$ is a relative velocity between the bodies of the investigated system; $\alpha_1 = \omega^2 m/k_2$, $\alpha_2 = \omega^2 J/k_2 r^2$, $\beta_1 = (k_1 + k_2)/k_2$, $\beta_2 = \mu_0 k_3/k_2$, $\beta_3 = (k_2 + k_3)/k_2$, $\eta_1 = c_1\omega/k_2$, $\eta_2 = c_2\omega\mu_0/k_2$, $\eta_{12} = \omega\,(c_1 + c_2)/k_2$ are the remaining parameters; ω is a periodicity of mass m. The friction force is described in the following manner:

$$\begin{cases} |T \le (1 - \beta_2 y_1 - \eta_2 y_2)\mu_0| & \text{for } v_{\rm rel} = 0, \\ T = \operatorname{sgn}(v_{\rm rel})\,(1 - \beta_2 y_1 - \eta_2 y_2)\mu_i & \text{for } v_{\rm rel} \neq 0, \end{cases} \tag{2}$$

where μ_i $(i = 1, 2)$ are friction coefficients defined for two various cases of our numerical analysis, i.e. the negative slope characteristic

$$\mu_1(v_{\rm rel}) = \frac{1}{1 + \gamma_1 |v_{\rm rel}|}, \tag{3}$$

and the Stribeck curve

$$\mu_2(v_{\rm rel}) = \frac{\mu_d}{\mu_0} + \left(1 - \frac{\mu_d}{\mu_0}\right) \exp\left(\frac{-\gamma_2\,|v_{\rm rel}|}{\mu_0 - \mu_d}\right), \tag{4}$$

where μ_0, μ_d are the coefficients of sticking and sliding (for $v_{\rm rel} \to \infty$) friction, respectively; γ_i $(i = 1, 2)$ are certain constant coefficients.

3. Numerical Analysis

In this paper the algorithm for numerical integration of the ODE including discontinuous term [see Eq. (2)] describing dry friction is applied. It is worth noticing that our self-excited system with friction

requires a special algorithm to avoid the problems occurring in the integration of Eq. (1). The used algorithm is based on the Hénon method [Hénon, 1982; Awrejcewicz & Olejnik, 2002] that proves to be extremely useful for locating and tracking of the stick to slip and slip to stick transitions in non-smooth systems.

Although the Hénon algorithm uses the Runge–Kutta method of fourth order, separate procedures can be introduced to detect the points belonging either to stick or to slip phases for both increasing and decreasing velocities. Special transformations are applied to eliminate jumps. The procedure is carried out with an automatically chosen step of numerical integration.

3.1. *Time histories*

It is obvious that the use of numerical methods can provide only approximate solutions of real trajectories of systems under analysis due to the finite step of numerical integrations and finite accuracy of the numbers used in the floating-point arithmetic. Nevertheless, if properly applied, numerical approximations prove sufficient for engineering purposes, which is important for our discontinuous system.

Duration of a transitional process depends on initial conditions and system parameters. In Fig. 2, one of the co-ordinates versus time is presented for

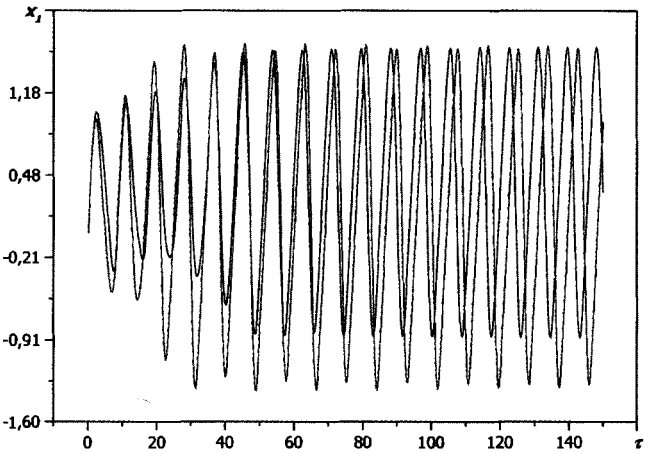

Fig. 2. Quickly stabilized periodic motion for μ_1 (black line) and μ_2 (red line) friction models for the parameters: $\alpha_1 = 3$, $\alpha_2 = 1.159$, $\beta_2 = 0.577$, $\beta_3 = 1.825$, $\eta_1 = \eta_2 = \eta_{12} = 0$, $\gamma_1 = 0.203$, $\gamma_2 = 0.813$, $v_b = 0.6$, $\mu_0 = 0.7$, $\mu_d = 0.18$ and initial conditions: $\tau_0 = 0$, $\tau_k = 150$, $x_1(0) = 0$, $x_2(0) = 0.6$, $y_1(0) = y_2(0) = 0$.

$\tau_0 = 0$. In this case, the masses are in the equilibrium positions, whereas their initial velocities are equal to the belt velocity. In practice, from the very beginning the system starts to move on an attractor. When the initial conditions are changed, duration of the transitional process becomes equal to about $\tau = 400$ (see Fig. 3). Our numerical analysis shows that in some cases the transitional state can

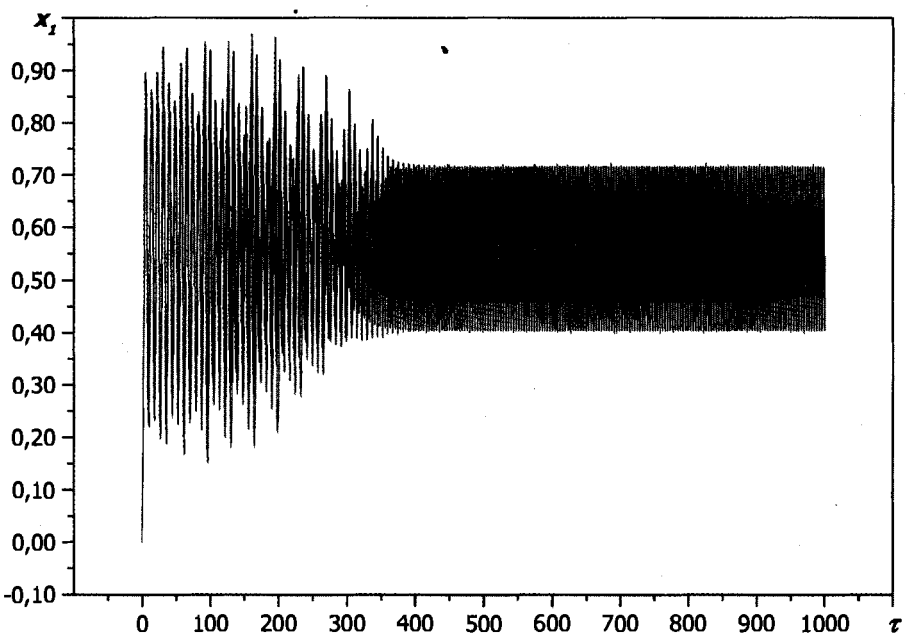

Fig. 3. Slowly stabilized periodic motion for μ_1 (black line) and μ_2 (red line) friction models for the parameters: $\alpha_1 = 2.4$, $\alpha_2 = 0.928$, $\beta_2 = 0.84$, $\beta_3 = 2.2$, $\eta_1 = \eta_2 = \eta_{12} = 0$, $\gamma_1 = 0.203$, $\gamma_2 = 0.813$, $v_b = 0.2$, $\mu_0 = 0.7$, $\mu_d = 0.6$ and initial conditions: $\tau_0 = 0$, $\tau_k = 150$, $x_1(0) = 0$, $x_2(0) = 0.2$, $y_1(0) = y_2(0) = 0$.

be many times longer, which may be of importance, especially in the engineering practice.

3.2. *Phase spaces*

The phase space of a dynamical system is a mathematical space in orthogonal coordinates that represents all of the variables which are necessary to determine a momentary state of the system. A typical projection of a trajectory associated with our system with friction is shown in Fig. 4. Two parts are easily distinguishable: a stick part (where $x_2 = v_b = 0.55$, which is represented by the horizontal line) and a slip part.

A more complicated motion is presented in Fig. 5. Time moments of an occurrence and duration of a stick are unpredictable. The mentioned phases appear with different velocities illustrated with small and large arcs in the phase plane. This means that the corresponding static friction force is smaller than an absolute value of the resulting horizontal forces.

3.3. *Poincaré sections*

Construction of a Poincaré section can be performed to replace investigations of the properties of the n-dimensional phase trajectory by an analysis of an $(n-1)$-dimensional discrete system. Different definitions are assumed for autonomous and nonautonomous dynamical systems. For our autonomous system the map construction is defined in the

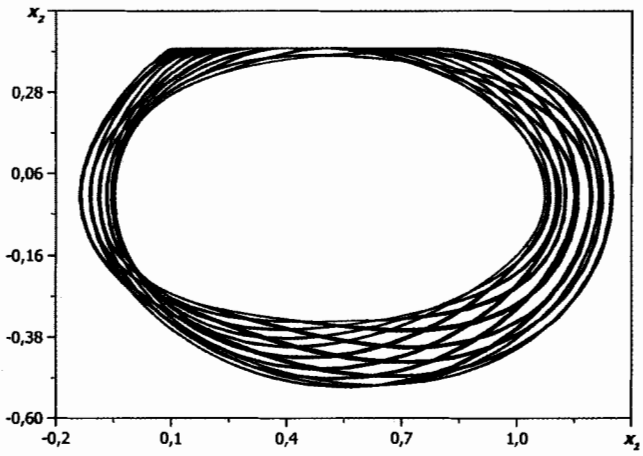

Fig. 5. Phase space projection of chaotic motion in (x_1, x_2) plane for μ_1 model for the parameters: $\alpha_1 = 2.83$, $\alpha_2 = 1.093$, $\beta_2 = 1.873$, $\beta_3 = 2.441$, $\eta_1 = \eta_2 = \eta_{12} = 0$, $\gamma_1 = 0.132$, $\gamma_2 = 0.66$, $v_b = 0.4$, $\mu_0 = 1.3$ and initial conditions: $\tau_0 = 2000$, $\tau_k = 4000$, $x_1(0) = 0$, $x_2(0) = -0.1$, $y_1(0) = y_2(0) = -0.1$.

following way:

$$\begin{aligned} &\text{if } x_{1,i-1} < x_{1,i} > x_{1,i+1} \Rightarrow y_{m,i} = [y_{1,i}, y_{2,i}], \\ &\text{if } y_{1,i-1} < y_{1,i} > y_{1,i+1} \Rightarrow x_{m,i} = [x_{1,i}, x_{2,i}], \end{aligned} \tag{5}$$

where $y_{m,i}$, $x_{m,i}$ are Poincaré map points of the angle body and the block, respectively; i denotes the iteration number of the solution of Eq. (1).

In what follows, we are going to show that our autonomous system can exhibit stick-slip periodic (Figs. 6 and 7), quasi-periodic (Fig. 8) as well as chaotic dynamics (Fig. 9).

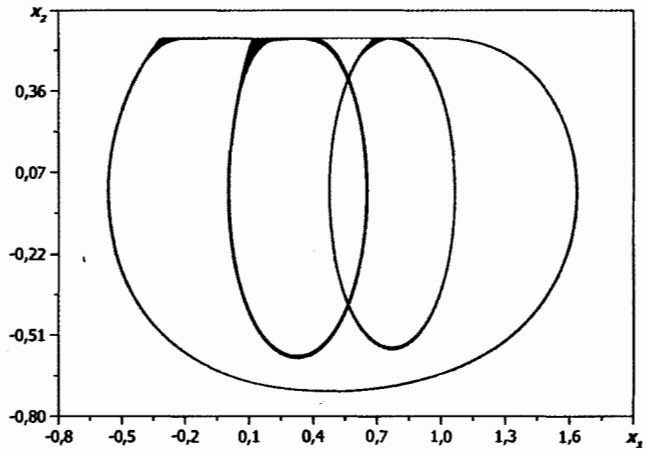

Fig. 4. Phase space projection of periodic motion in (x_1, x_2) plane for μ_1 (black line) and μ_2 ($\mu_d = 1.25$, red line, $\mu_d = 0.3$, blue line) models for the parameters: $\alpha_1 = 2.4$, $\alpha_2 = 0.927$, $\beta_2 = 2.304$, $\beta_3 = 2.8$, $\eta_1 = \eta_2 = \eta_{12} = 0$, $\gamma_1 = 0.289$, $\gamma_2 = 1$, $v_b = 0.55$, $\mu_0 = 1.28$ and initial conditions: $\tau_0 = 3000$, $\tau_k = 3500$, $x_1(0) = 0$, $x_2(0) = -0.1$, $y_1(0) = y_2(0) = -0.1$.

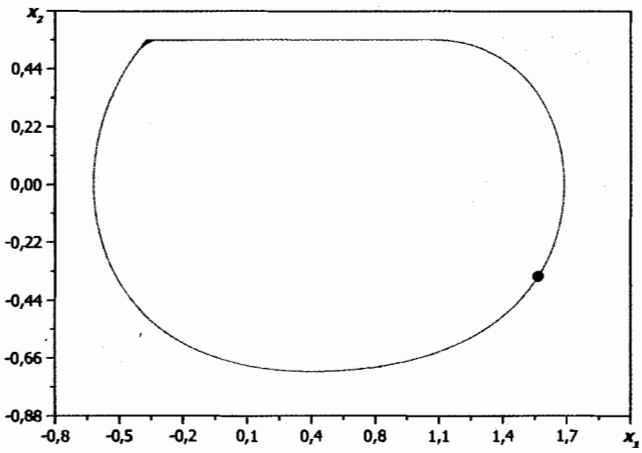

Fig. 6. Phase space projection of 1-periodic motion of the block in (x_1, x_2)-plane and its Poincaré section (red circle) for μ_1 model for the parameters: $\alpha_1 = 2.4$, $\alpha_2 = 0.927$, $\beta_2 = 2.304$, $\beta_3 = 2.8$, $\eta_1 = \eta_2 = \eta_{12} = 0$, $\gamma_1 = 0.289$, $\gamma_2 = 0.999$, $v_b = 0.55$, $\mu_0 = 1.28$ and initial conditions: $\tau_0 = 4000$, $\tau_k = 4300$, $x_1(0) = 0$, $x_2(0) = -0.1$, $y_1(0) = 0$, $y_2(0) = -0.1$.

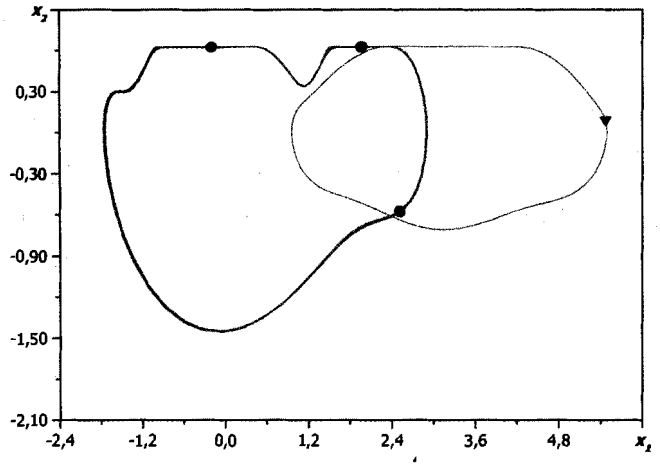

Fig. 7. Phase space projection of periodic motions of the block in (x_1, x_2)-plane and their Poincaré section for μ_1 (blue circle) and μ_2 (red triangle) model for the parameters: $\alpha_1 = 2.5$, $\alpha_2 = 0.966$, $\beta_2 = 3.712$, $\beta_3 = 2.125$, $\eta_1 = \eta_2 = \eta_{12} = 0$, $\gamma_1 = 0.577$, $\gamma_2 = 2.047$, $v_b = 0.63$, $\mu_0 = 3.3$, $\mu_d = 0.3$ and initial conditions: $\tau_0 = 700$, $\tau_k = 1000$, $x_1(0) = 0$, $x_2(0) = -0.1$, $y_1(0) = 0$, $y_2(0) = -0.1$.

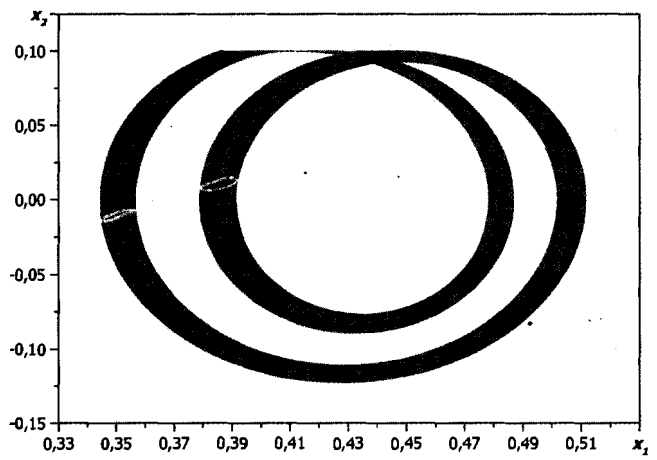

Fig. 8. Phase space projection of quasi-periodic motion of the block in (x_1, x_2)-plane and its Poincaré section for μ_1 (yellow curve) model for the parameters: $\alpha_1 = 2.874$, $\alpha_2 = 1.111$, $\beta_2 = 0.412$, $\beta_3 = 2.472$, $\eta_1 = \eta_2 = \eta_{12} = 0$, $\gamma_1 = 0.035$, $\gamma_2 = 0.141$, $v_b = 0.1$, $\mu_0 = 0.28$ and initial conditions: $\tau_0 = 4000$, $\tau_k = 7000$, $x_1(0) = x_2(0) = 0$, $y_1(0) = y_2(0) = 0$.

Points of the Poincaré sections presented in Figs. 6–9 are matched by solid black circles against the background of their phase spaces. Moreover, Fig. 8 presents attractors in the shape of black closed curves confirming occurrence of a quasi-periodic motion. An unpredictable form of the chaotic attractor is presented in Fig. 9. Long-time solution provides location of randomized points.

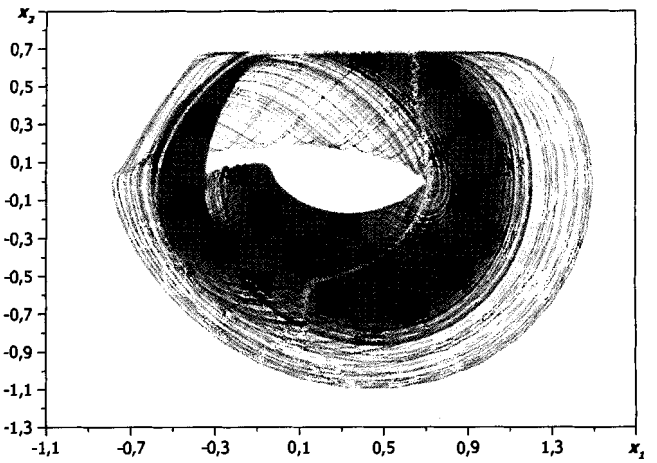

Fig. 9. Phase space projection of chaotic motion of the block in (x_1, x_2)-plane and its Poincaré section for μ_1 (yellow points) model for the parameters: $\alpha_1 = 4.5$, $\alpha_2 = 1.739$, $\beta_2 = 6.766$, $\beta_3 = 3.333$, $\eta_1 = \eta_2 = \eta_{12} = 0$, $\gamma_1 = 0.976$, $\gamma_2 = 3.551$, $v_b = 0.689$, $\mu_0 = 2.9$ and initial conditions: $\tau_0 = 2000$, $\tau_k = 20000$, $x_1(0) = 0$, $x_2(0) = -0.1$, $y_1(0) = 0$, $y_2(0) = -0.1$.

3.4. *Bifurcation diagrams*

Bifurcation diagrams are constructed by changing a parameter in the interval [0.2, 0.7] with step 0.001, wherefrom 500 Poincaré maps are obtained. Then,

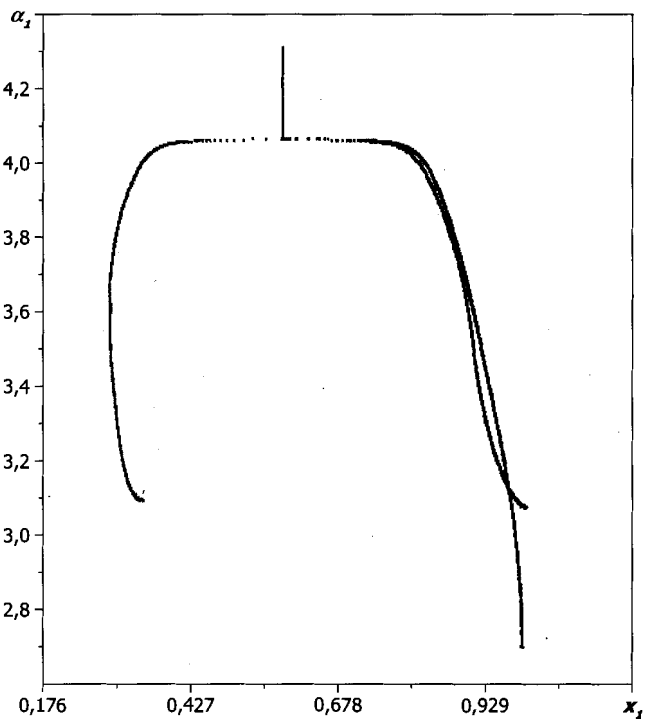

Fig. 10. Bifurcation diagram of $\alpha_1 \in (2.72; 4.32)$ parameter versus x_1 displacement in the time interval from $\tau_0 = 1000$ to $\tau_k = 51000$ (remaining parameters are as in Fig. 2).

one of the phase axes is selected and all results are presented versus the parameter. Another way is to increase parameter values by changing the initial conditions. In this case, we leave an attractor, contrary to the first case in which we stayed on an attractor all the time.

An example of the bifurcation diagram is shown in Fig. 10. Beginning from the smallest considered values of α_1 we observe the one-periodic motion, but for $\alpha_1 \approx 3.1$ a period tripled bifurcation with an increase of α_1 occurs. In the vicinity of bifurcation point $\alpha_1 \approx 4.0$, the period tripled bifurcation with a decrease of the bifurcation parameter is observed once again. It should be emphasized that for a large interval of changes of the bifurcation parameter only the periodic motion can be reached by our analyzed system.

An interesting example of more complex bifurcations is shown in Fig. 11. It may be traced how the successive period doubling (accompanying the decrease of α_1 parameter) leads to a chaotic motion, which exists for $\alpha_1 \approx 2.9$. Additionally, period-n windows for $\alpha_1 \approx \{3.15, 3.05, 2.95\}$ are reported.

3.5. *Lagrange interpolation and Lyapunov exponents*

The Lagrange polynomial scheme is applied to estimate Lyapunov exponents numerically from a

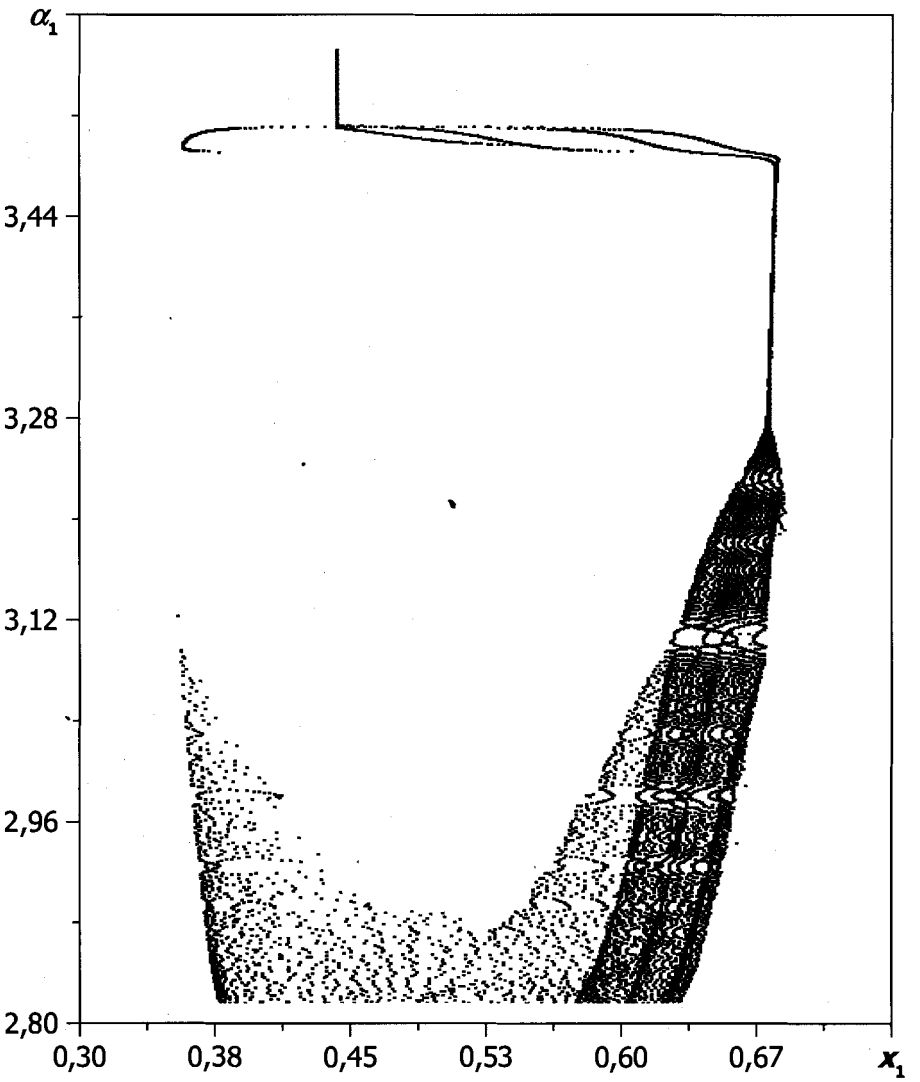

Fig. 11. Bifurcation diagram of $\alpha_1 \in (2.83; 3.58)$ parameter versus x_1 displacement for μ_2 model for the parameters: $\alpha_2 = 1.093$, $\beta_2 = 1.729$, $\beta_3 = 2.441$, $\eta_1 = \eta_2 = \eta_{12} = 0$, $\gamma_1 = 0.152$, $\gamma_2 = 0.609$, $v_b = 0.1$, $\mu_0 = 1.2$, $\mu_d = 0.3$ and initial conditions: $\tau_0 = 1000$, $\tau_k = 51000$, $x_1(0) = 0$, $x_2(0) = 0.1$, $y_1(0) = y_2(0) = 0$.

stored time series in hard computer memory. The time series with a variable time step of the Hénon integration procedure is obtained by solving Eq. (1). The Lagrange interpolation is performed for each time history of the phase coordinates of the system. The series is then interpolated using standard Lagrange interpolation scheme by a new one, where points are distributed in equal intervals of time. The latter ones are then used to estimate Lyapunov exponents. The convergence of Lyapunov's exponents versus iterations n for a chaotic attractor are illustrated in Fig. 12.

A good convergence is achieved after about $n = 500$ iterations of the computation procedure. The friction still affects the presented convergence form in an essential way. Lyapunov exponents have been estimated for Figs. 6–9 and summarized in Table 1.

In this table, R denotes a relation between the number of points of the trajectory solved by means of the Hénon method and its Lagrange interpolated equivalent.

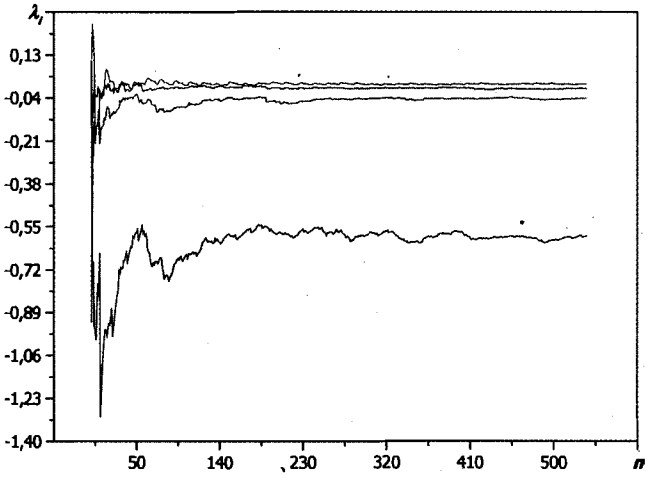

Fig. 12. Lyapunov exponents λ_i convergence for the chaotic motion shown in Fig. 9.

Table 1. Lyapunov exponents spectrum for the motions illustrated in Figs. 6–9.

	Lyapunov Exponents					
Fig.	λ_1	λ_2	λ_3	λ_4	R	$\tau[\cdot 10^3]$
6	**−0.0047**	−0.0174	−0.0480	−0.4566	30	3–12
7	**−0.0031**	−0.0419	−0.1521	−0.3645	28	3–12
8	**+0.0001**	**−0.0002**	−0.0733	−0.8381	23	4–11
9	+0.0146	**−0.0030**	−0.0400	−0.5869	21	2–10

4. Experimental Investigations

In this section, the numerical analysis is supported by experimental investigations. For that purpose a laboratory rig designed for observations and experimental research of the friction effects including the friction force measurement is constructed. Photos of the rig are presented in Fig. 13.

The general view, component parts and some connectors, like coil springs, correspond to the elements schematically indicated and presented in Fig. 1.

Displacement of the block and the angle of rotation are measured using a laser proximity switch and a Hall-effect device, which guaranties a nonsticking method of the measurement. Both provide the linear dependency of the measured quantity versus the analogue voltage output. Measurement instruments connected through PCI computer card to LabView software enable the dynamic acquisition of the two measured signals. Disturbances of the entire construction, noise in electrical circuits, and other additional maintenances influence significantly the accuracy of any measured signals. Therefore, some signals are filtered digitally (elliptic topology) and a real differentiation preventing formation of high peaks is applied.

4.1. *Results of experimental measurements*

Measurement results are obtained following the methodology described in Sec. 3. The examples of time characteristics of state variables are shown in Fig. 14.

A characteristic positive slope (slip phase of the block) of the time history and a negative slope (stick phase of the block) can be seen in Fig. 14(a). A time dependency of velocity of the block is presented in Fig. 14(b). There are some time intervals between nodes where velocity is almost constant and equal to the belt velocity. This happens if the considered block is in the stick phase. Otherwise, the stick phase can be observed on a time history graph of acceleration, where some of the intervals (at the zero value of velocity) are parallel to t-axis.

The phase planes give an opportunity to explore the dynamics of the investigated system more comprehensively. The well-known shapes of phase curves usually visible in the stick-slip motion are presented in Figs. 15(a) and 15(b). The stick (almost straight lines) and slip (arcs connecting

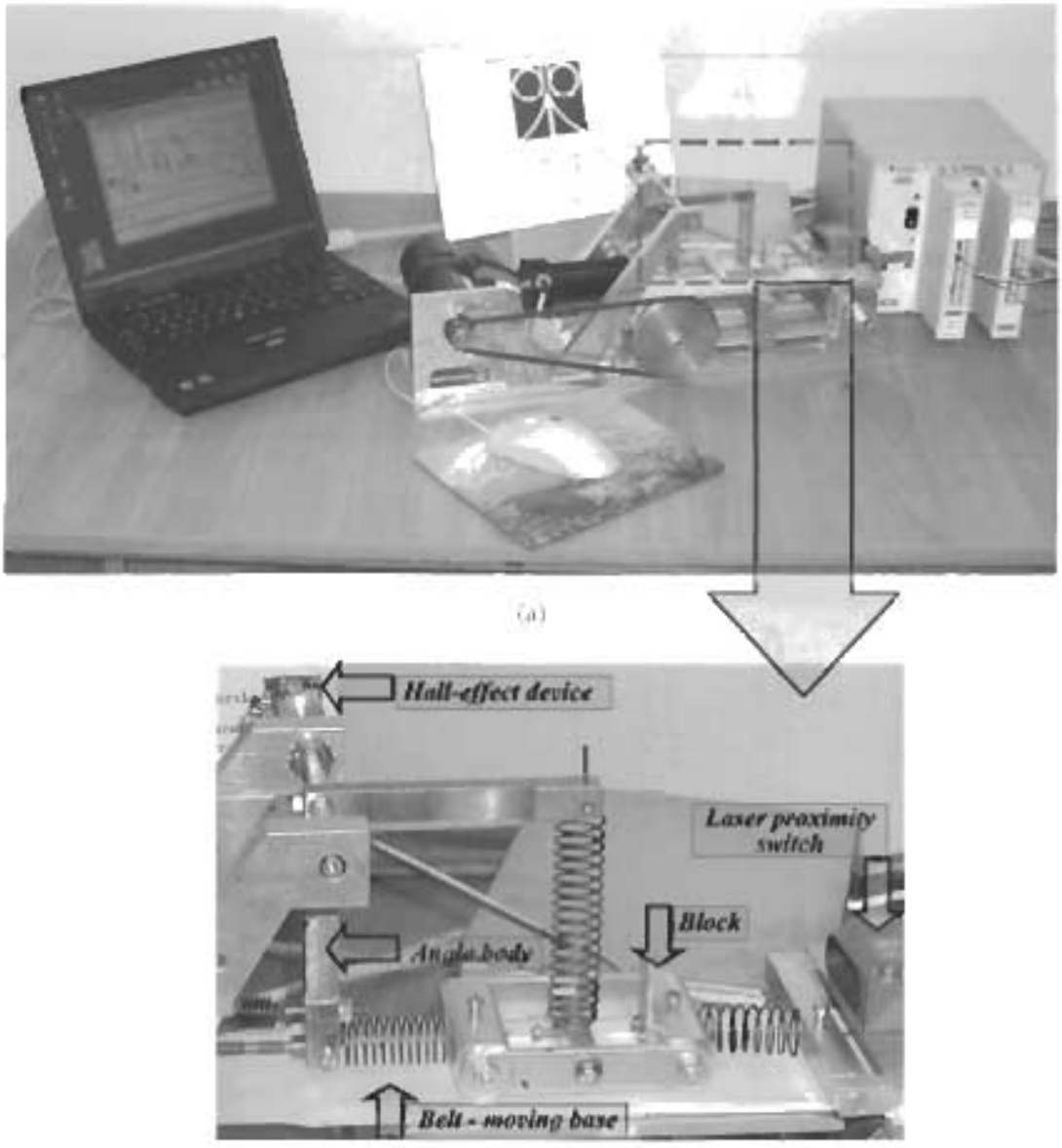

(a)

(b)

Fig. 13. The laboratory rig (a) general view (b) its vibratory subsystem

the ends of the straight lines) phases can be easily observed.

4.2. *Friction force model*

Appropriately transformed equations of motion [see Eq. (1)] can be used to calculate the friction force after the state variables of the investigated system have been measured in real time. Characteristics of the friction force versus the relative velocity between the belt and the block for positive and negative velocities of the belt are shown in Fig. 16.

It can be observed that the zones occupied by the closed functions of the friction model differ significantly. It is a regularity since the angle body causes reinforcement of the friction force for the positive velocity of the moving base [see Fig. 1 Fig. 13(b)]. This explains why the T_+ and T_- friction force characteristics are described by linearly and exponentially (of second order) decaying functions, respectively. The friction force model represented by the solid red curve and indicated in Fig. 16 is separated from the real friction force dependencies for all relative velocities v_{rel} as illustrated in Figs. 17 and 18.

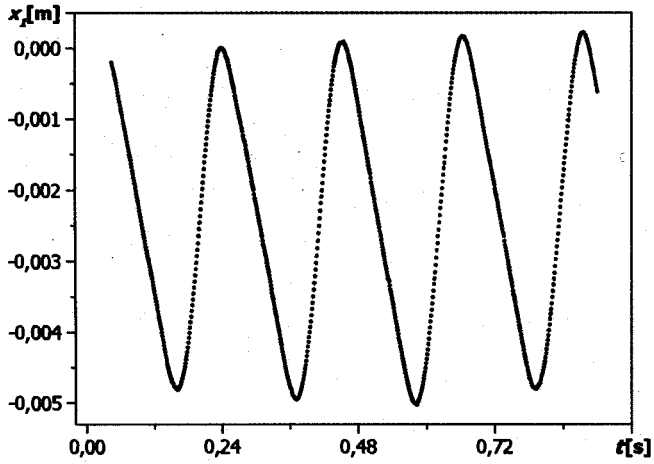

(a)

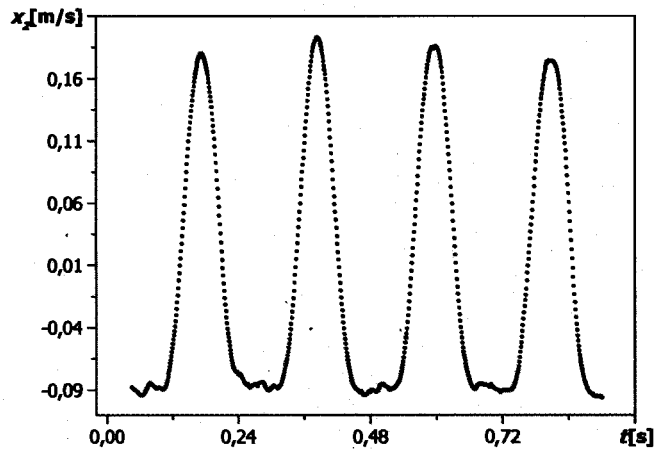

(b)

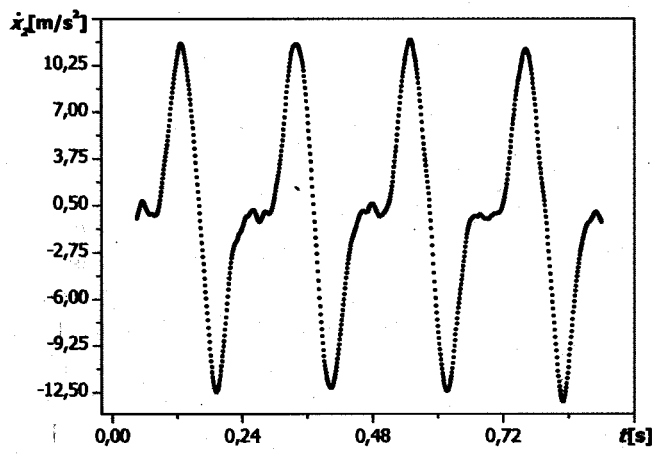

(c)

Fig. 14. Real time histories of (a) displacement x_1, (b) velocity x_2 and (c) acceleration $\dot{x}_2$ of the block for velocity of the belt $v_b = -0.13\,\mathrm{m/s}$.

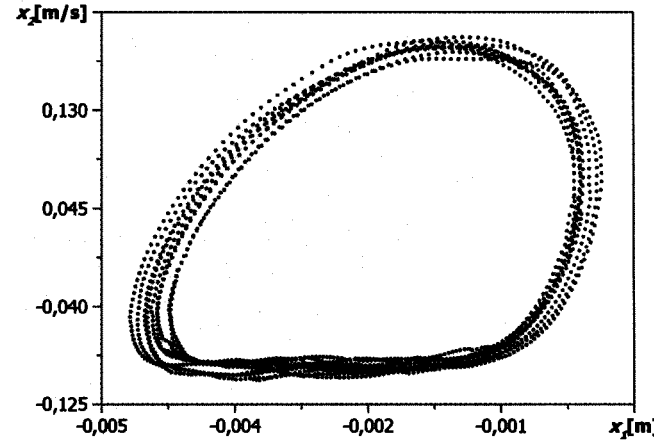

(a)

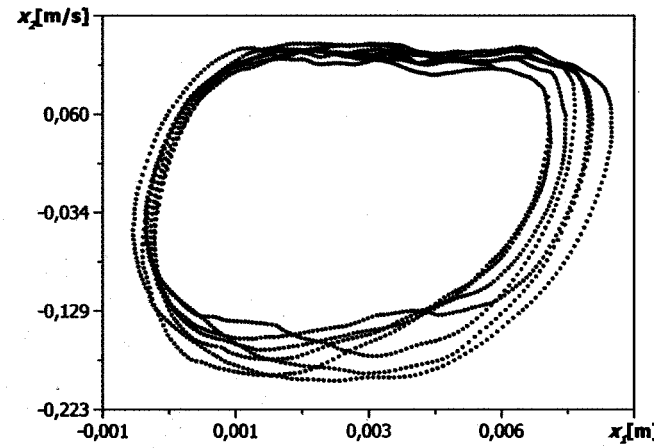

(b)

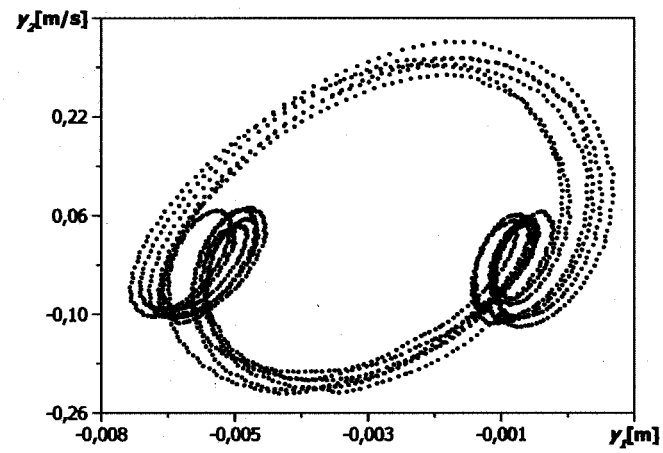

(c)

Fig. 15. Phase planes of the block for (a) $v_b < 0$, (b) $v_b > 0$, and the phase plane of (c) the angle body for $v_b > 0$.

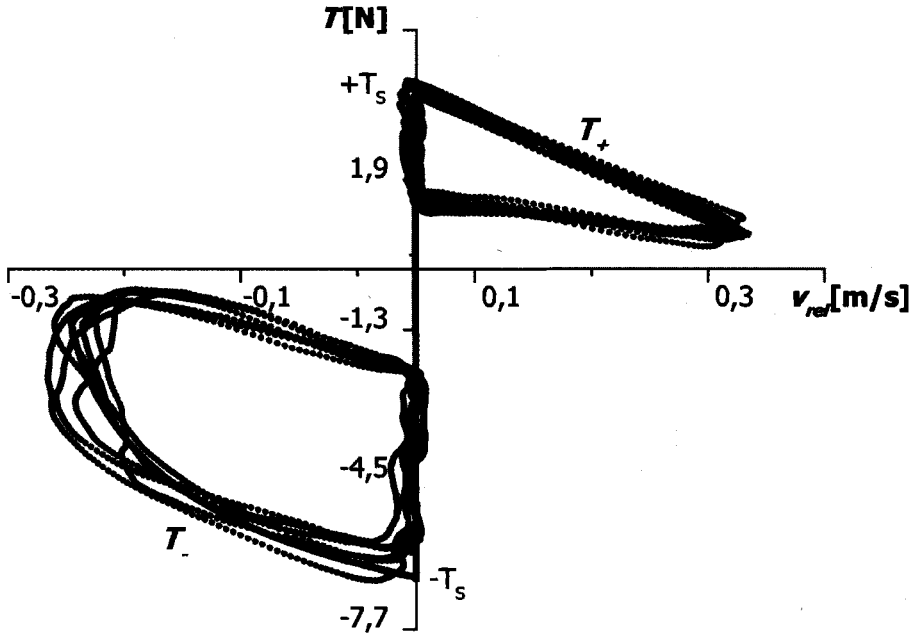

Fig. 16. Friction force characteristics for positive (T_+) and negative (T_-) relative velocities.

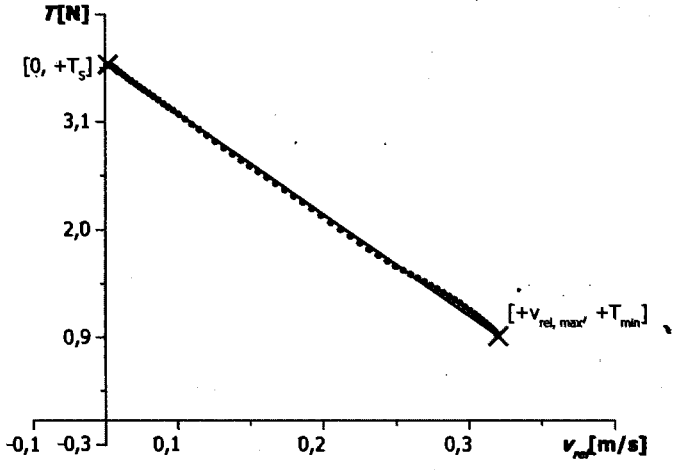

Fig. 17. Linear fitting (solid black line) of the branch of the real friction force characteristics (solid red points) for the positive relative velocity.

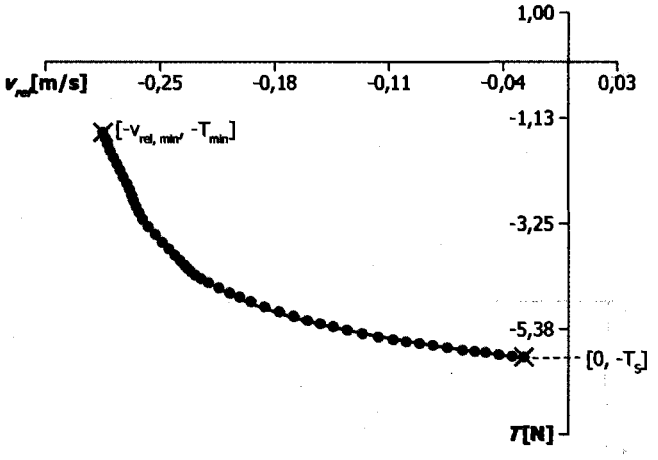

Fig. 18. Exponential fitting (solid black line) of the branch of the real friction force characteristics (solid red points) for the negative relative velocity.

In the case of the T_+ branch, the equation of the friction force dependence describing the friction force model for the positive relative velocity have the following form:

$$T_+ = T_s - |v_{\mathrm{rel}}| \frac{T_s - T_{\min}}{v_{\mathrm{rel,\,max}}}, \tag{6}$$

where T_s is a static friction force, $v_{\mathrm{rel,\,max}}$ is a maximum positive relative velocity. The T_- branch can be described by an exponentially decaying function of second order describing the friction force model for the negative relative velocity of the following form:

$$T_- = T_s + A_1 \exp\left(-\frac{|v_{\mathrm{rel}}| - v_{\mathrm{rel,\,min}}}{t_1}\right) + A_2\left(-\frac{|v_{\mathrm{rel}}| - v_{\mathrm{rel,\,min}}}{t_2}\right), \tag{7}$$

where $v_{\mathrm{rel,\,min}}$ is a maximum negative velocity, A_1, A_2, t_1, t_2 are constant values. The main multivalued function describing friction force changes (red line in Fig. 16) occurring in our investigated 2-DOF

system with a variable normal force is determined from the following equation:

$$T = \begin{cases} \operatorname{sgn}(v_{\mathrm{rel}})\, T_+ & \text{if } v_{\mathrm{rel}} > 0, \\ \operatorname{sgn}(v_{\mathrm{rel}})\, T_- & \text{if } v_{\mathrm{rel}} < 0, \\ |T_S| & \text{if } v_{\mathrm{rel}} = 0. \end{cases} \tag{8}$$

4.3. *Comparisons*

The friction force model given by Eq. (8) is transformed to a nondimensional one, and then a numerical analysis based on the T_+ and T_- friction force characteristics is carried out. The parameters of the two models are obtained by both measurement and identification: $T_s = 3.63$, $T_{\min} = 0.86$, $v_{\mathrm{rel,max}} = 0.27$ (T_+ branch); $T_s = -5.94$, $T_{\min} = -1.42$, $-v_{\mathrm{rel,max}} = 0.28$, $A_1 = 3.23453$, $A_2 = 2.87362$, $t_1 = 0.0342$, $t_2 = 0.30529$ (T_- branch). The numerical analysis with implementation of the introduced friction force dependency yielded the results presented in Fig. 19.

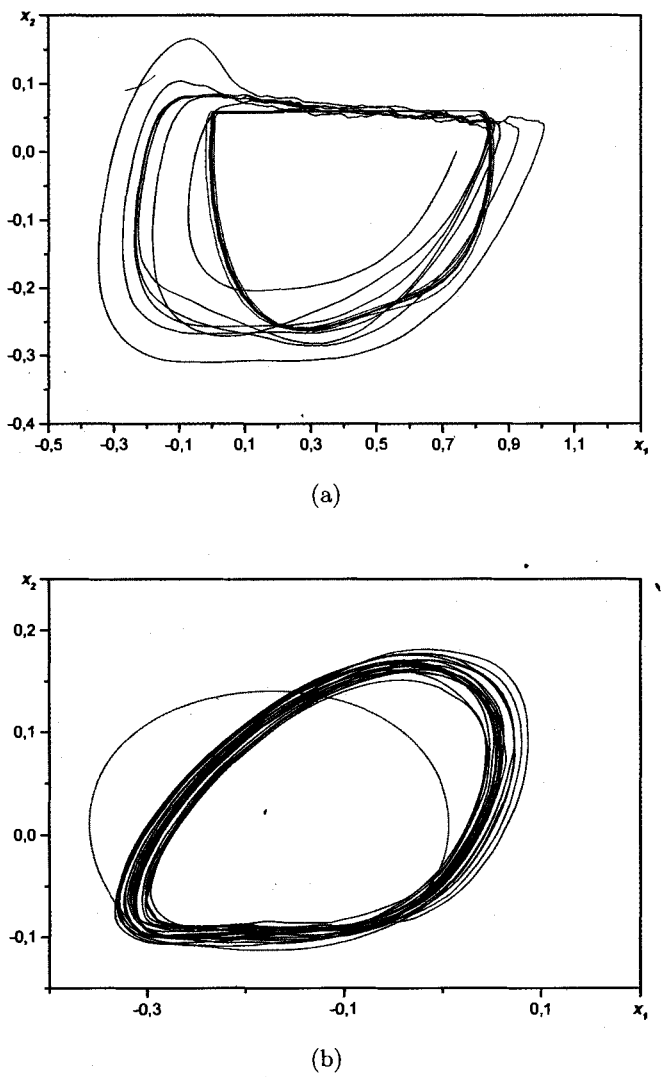

Fig. 19. Verification of the results obtained via computer simulation (red line) with experimental measurement of state variables (black line) of the analyzed system: friction force model: (a) T_-, (b) T_+; parameters: $\alpha_1 = 1.87$, $\alpha_2 = 0.72$, $\beta_1 = 2.87$, $\beta_2 = 1.62$, $\beta_3 = 2.47$, $\eta_1 = \eta_2 = \eta_{12} = 0$, $v_b = 0.06$, $\mu_0 = 1.1$; initial conditions: $t_0 = 400$, $t_k = 5000$, $x_1(0) = 0$, $x_2(0) = 0$, $y_1(0) = y_2(0) = 0$.

The numerical trajectory (red line) illustrated in Fig. 19(a) is satisfactorily close to its experimental counterpart recorded for the investigated dynamical system. The sticking velocity is almost the same, but in the sliding phase some distinguishable differences are observed. T_- friction force model can be used after the friction effects occurring in the systems with the variable normal force acting between cooperated surfaces have been analyzed.

A significant difference between the trajectories under consideration [cf. Fig. 19(b)] is visible, but the sticking phase still coincides for the positive relative velocity. The comparison of the results with those in Fig. 19(b) shows nonsymmetry of the system under analysis, which is the information of considerable usefulness.

5. Conclusions

The 2-DOF self-excited system with friction is analyzed using numerical methods. A special numerical scheme based on the Hénon approach and exhibiting good suitability for investigations of nonsmooth dynamical systems is applied. Many interesting dynamical nonlinear behaviors are reported and analyzed, including stick-slip periodic (Figs. 4, 6 and 7), quasi-periodic (Fig. 8) and chaotic (Fig. 9) motions. In the analysis, all standard techniques are applied, i.e. time histories, phase planes, Poincaré maps, bifurcation diagrams and the Lyapunov exponents. The calculation of Lyapunov's exponents from an interpolated time series offers sufficient accuracy and correct values of its spectrum. The expected estimation accuracy of the Lyapunov exponents for each type of the motion yields different R relations between the number of the trajectory points solved by the Hénon method and its equivalent Lagrange interpolation.

In addition, the numerical analysis is supported by the investigation of a real laboratory object modeling the feedback reinforcement of the friction force (model of T_- branch) and the friction force without the feedback (model of T_+ branch). The numerical solution (red curve) obtained using the

T_- branch model has not proved a transition, which can be observed in our experimental measurement (black curve). The sticking velocity is almost the same, but in the sliding phase some distinguishable differences are observed. It is suggested that the T_- friction force model should be used after an analysis of the friction effects occurring in the systems where the normal force acting between cooperated surfaces is fluctuated. Application of the T_+ branch friction force model leads to rapid entries on the\stick phase and rather smooth backslides from it [see red line in Fig. 19(b)].

To conclude, a new idea for the friction pair modeling using both laboratory equipment and numerical simulations is proposed allowing for observation and control of the friction force. The experimental data are compared with those obtained via numerical simulations showing good agreement.

Acknowledgment

This work has been supported by the Polish State Committee for Scientific Research (grant No 4 T11F 005 22).

References

Altpeter, F., Ghorbel, F. & Longchamp, R. [1998] "Relationship between two friction models: A singular perturbation approach," *Proc. 37th IEEE Conf. Decision and Control*, pp. 1572–1574.

Andreaus, U. & Casini, P. [2001] "Dynamics of friction oscillators excited by a moving base and/or driving force," *J. Sound Vibr.* **245**, 685–699.

Antunes, J., Axisa, F., Beaufils, B. & Guilbaud, B. [1988] "Coulomb friction modeling in numerical simulations of vibrations and wear work rate of tube bundles," *J. Fluids Struct.* **4**, 287–304.

Armstrong-Hélouvry, B. [1992] "A perturbation analysis of stick-slip," *Trans. ASME Friction-Induced Vibr. Chat. Squ. Chaos* **49**, 41–48.

Awrejcewicz, J. & Delfs, J. [1990a] "Dynamics of a self-excited stick-slip oscillator with two degrees of freedom, Part I, Investigation of equilibria," *European J. Mech. A/Sol.* **9**, 269–282.

Awrejcewicz, J. & Delfs, J. [1990b] "Dynamics of a self-excited stick-slip oscillator with two degrees of freedom, Part II, Slip-stick, slip-slip, stick-slip transitions, periodic and chaotic orbits," *European J. Mech. A/Sol.* **9**, 397–418.

Awrejcewicz, J. [1996] *Deterministic Oscillations of Lumped Systems* (WNT, Warsaw, in Polish).

Awrejcewicz, J. & Holicke, M. M. [1999] "Melnikov's method and stick-slip chaotic oscillations in very weakly forced mechanical systems," *Int. J. Bifurcation and Chaos* **9**, 505–518.

Awrejcewicz, J. & Olejnik, P. [2002] "Calculating Lyapunov exponents from an interpolated time series," *XX Sym. Vib. Phys. Systems Poznań-Błażejewko*, pp. 94–95.

Awrejcewicz, J. & Olejnik, P. [2003] "Improvement of the Lyapunov exponents computations by time series extension," *Proc. 11th World Cong. Mechanism and Machine Science*, to appear.

Bliman, P.-A. & Sorine, M. [1995] "Easy-to-use realistic dry friction models for automatic control," *Proc. 3rd Euro. Control Conf.*, pp. 3788–3794.

Bogacz, R. & Ryczek, B. [1997] "Dry friction self-excited vibrations analysis and experiment," *Eng. Trans.* **45**, 487–504.

Bowden, F. P. & Tabor, D. [1954] *Friction and Lubrication* (Oxford University Press).

Brandl, M. & Pfeiffer, F. [1999] "Tribometer for dry friction measurement," *Proc. ASME Des. Eng. Tech. Conf.*, DETC99/VIB-8353.

Brogliato, B. [1996] *Nonsmooth Impact Mechanics* (Springer-Verlag, London).

Canudas de Vit, C., Olsson, H., Åström, K. J. & Lischinsky, P. [1995] "A new model for control of systems with friction," *Proc. 34th IEEE Trans. Autom. Contr.* **40**, 419–425.

Dahl, P. R. [1976] "Solid friction damping of mechanical vibrations," *J. AIAA* **14**, 1675–1682.

Feeny, B., Guran, A., Hinrichs, N. & Popp, K. [1998] "A historical review on dry friction and stick-slip phenomena," *Appl. Mech. Rev.* **51**, 321–341.

Friedland, B. & Park, Y.-J. [1991] "On adaptive friction compensation," *Proc. 30th IEEE Conf. Decision and Control*, pp. 2899–2902.

Galvanetto, U., Bishop, S. R. & Briseghella, L. [1995] "Mechanical stick-slip vibrations," *Int. J. Bifurcation and Chaos* **5**, 637–651.

Hénon, M. [1982] "On the numerical computation of Poincaré maps," *Physica* **D5**, 412–413.

Ibrahim, R. A. [1992] "Mechanics of friction," *Trans. ASME Friction-Induced Vibr. Chat. Squ. Chaos* **49**, 107–122.

Karnop, D. [1985] "Computer simulation of stick-slip friction in mechanical dynamic systems," *Trans. ASME J. Dyn. Syst. Contr.* **107**, 100–103.

Kunze, M. [2000] *Non-Smooth Dynamical System*, Lecture Notes in Mathematics, Vol. 1744 (Springer-Verlag, Berlin).

Makris, N. & Constantinou, M. C. [1991] "Analysis of motion resisted by friction. Part I: Constant Coulomb and linear/Coulomb friction," *Mech. Struct. Mach.* **19**, 477–500.

Monteiro Marques, M. D. P. [1994] "An existence, uniqueness and regularity study of the dynamics of systems with one-dimensional friction," *European J. Mech. A/Sol.* **13**, 277–306.

Oden, J. T. & Martins, J. A. C. [1985] "Models and computation methods for dynamic friction phenomena," *Comp. Meth. Appl. Mech. Eng.* **52**, 527–634.

Popp, K., Hinrichs, N. & Oestreich, M. [1996] "Analysis of a self-excited friction oscillator with external excitation," in *Dynamics with Friction*, eds. Guran, A., Pfeiffer, F. & Popp, K., pp. 1–35.

Singer, I. L. & Pollock, H. M. [1992] *Fundamentals of Friction: Macroscopic and Microscopic Processes* (Kluwer Academic Publishers, Dordrecht).

Tan, X. & Rogers, R. J. [1996] "Dynamic friction modeling in heat exchanger tube simulations," *Trans. ASME Friction-Induced Vibr. Chat. Squ. Chaos* **328**, 347–358.

Van Wyk, M. A. & Steeb, W.-H. [1997] *Chaos in Electronics* (Kluwer Academic Publishing).

Wolf, A., Swift, J. B., Swinney, H. L. & Vastano, J. A. [1985] "Determining Lyapunov exponents from a time series," *Physica* **D16**, 285–317.